

# Long-circulating QD probes for in-vivo tumor imaging

Xiaohu Gao and Shuming Nie

Departments of Biomedical Engineering, Chemistry, Hematology and Oncology, and the Winship Cancer Institute, Emory University and Georgia Institute of Technology, 1639 Pierce Drive, Suite 2001, Atlanta, GA 30322, USA.

Correspondence should be addressed to S. N. ([snie@emory.edu](mailto:snie@emory.edu))

## ABSTRACT

Biocompatible semiconductor quantum dot (QD) probes with extended plasma circulating times have been developed for cancer imaging in living animals. The structural design involves encapsulating luminescent QDs with a triblock copolymer, and linking this amphiphilic polymer to multiple poly(ethylene glycol) (PEG) molecules. *In vitro* histology and *in vivo* imaging studies indicate that the QD probes can be delivered to tumor sites by enhanced permeation and retention. Using both systemic injection of long-circulating QD probes and subcutaneous injection of QD-tagged microbeads, we have achieved sensitive and multicolor fluorescence imaging of cancer cells under *in vivo* conditions. These results raise new possibilities for ultrasensitive and multiplexed imaging of molecular targets *in vivo*.

**Keywords:** quantum dots, fluorescence, molecular imaging, targeting, nanoparticles, probes, multicolor, long circulating

## 1. INTRODUCTION

The development of high-sensitivity and high-specificity probes beyond the intrinsic limitations of organic dyes and fluorescent proteins is of considerable interest to many areas of research, ranging from molecular and cellular biology to molecular imaging and medical diagnostics. Recent advances have shown that nanometer-sized semiconductor particles can be covalently linked with biorecognition molecules such as peptides, antibodies, nucleic acids, or small-molecule ligands for applications as fluorescent probes<sup>1-13</sup>. In comparison with organic fluorophores, these quantum-confined particles or quantum dots (QDs) exhibit unique optical and electronic properties, such as size- and composition-tunable fluorescence emission from visible to infrared wavelengths, large absorption coefficients across a wide spectral range, and very high levels of brightness and photostability<sup>14,15</sup>. Due to their broad excitation profiles and narrow/symmetric emission spectra, high-quality QDs are also well suited for optical multiplexing, in which multiple colors and intensities are combined to encode genes, proteins, or small-molecule libraries<sup>16,17</sup>.

Despite their relatively large hydrodynamic radii (10–15 nm), recent research has shown that bioconjugated QD probes do not suffer from serious binding kinetic or steric-hindrance problems<sup>6-12</sup>. In this “mesoscopic” size range, QDs also have more surface areas and functionalities that can be used for linking to multiple diagnostic (e.g., radioisotopic or magnetic) and therapeutic (e.g., anticancer) agents. Indeed, Josephson, Weissleder and coworkers<sup>18</sup> have developed dual magnetic and optical probes by using similarly sized iron oxide nanoparticles, a magnetic contrast agent that is currently evaluated for clinical use.

These properties have opened new possibilities for advanced molecular and cellular imaging as well as for ultrasensitive bioassays and diagnostics<sup>19</sup>. Akerman et al.<sup>5</sup> first reported the use of QD-peptide conjugates to target tumor vasculatures, but the QD probes were not detected in living animals. Nonetheless, their *in vitro* histological results revealed that QDs homed to tumor vessels guided by the peptides and were able to escape clearance by the reticuloendothelial system (RES). In a significant improvement, Dubertret et al.<sup>6</sup> encapsulated QDs in phospholipids micelles, and injected these biocompatible dots into frog oocyte cells for real-time tracking of

embryonic development. With two-photon laser excitation, Larson et al.<sup>9</sup> demonstrated the use of quantum dots as a fluorescent blood tracer to image small vasculatures close to the skin surface. Theoretical modeling studies have been reported by Lim et al.<sup>20</sup>, indicating that two spectral windows could be available for *in vivo* QD imaging (one at 700–900 nm and another at 1200–1600 nm). Quantum dots have also been used as stable fluorescent tracers for RES uptake studies and lymph node mapping in living animals<sup>21,22</sup>. Most recently, we have reported a new class of multifunctional QD probes for simultaneous targeting and imaging of prostate tumors in live animals using antibody-conjugated QDs<sup>23</sup>.

In this paper, we report the development of PEG coated long-circulating QD probes that are highly biocompatible and suitable for *in vivo* tumor imaging. In comparison with simple water-soluble QDs, the PEG coated dots are stable in a broad range of pH values and salt concentrations. Due to their unique structural and surface properties, this new type of fluorescence contrast reagent is able to stay in the blood stream for an extended period of time, and is able to accumulate at tumor sites through the enhanced permeation and retention (EPR). These long-circulating probes are useful in broad tumor imaging applications because angiogenesis and disordered vasculatures are a common feature in many types of solid tumors. We have examined their biodistribution, RES uptake, cellular toxicity, and pharmacokinetics in cells and animal models. Using QD-encoded microbeads injected subcutaneously into living animals, we have achieved excellent detection sensitivity and multicolor capability. These results open new possibilities for ultrasensitive and simultaneous imaging of multiple biomarkers involved in cancer metastasis and invasion.

## 2. EXPERIMENTAL

Animal use protocols were reviewed and approved by the Institutional Animal Care and Use Committee of Emory University.

**2.1 Materials.** Except noted otherwise, all chemicals and biochemicals were purchased from Sigma-Aldrich (St. Louis, MO) and were used without further purification. mPEG-NH<sub>2</sub> with a molecular weight of 5,000 was purchased from SunBio (Korea) or Nektar Therapeutics (San Carlos, CA).

**2.2 Quantum dot synthesis.** To prepare high-quality QDs suitable for block polymer encapsulation and *in-vivo* imaging, we synthesized core CdSe nanocrystals by using the procedure of Peng et al. and coated the core particles with a CdS shell (1-nm thick) by the procedure of Hines et al.<sup>24,25</sup>. Briefly, cadmium oxide (CdO, 0.2 millimole) precursor was first dissolved in 0.5 g stearic acid and 2 g TOPO with heating under argon flow. After formation of a clear solution, the reaction was cooled down to room temperature, followed by addition of 2 g HDA, which was then heated back to 250 °C under argon for 10 minutes. The temperature was briefly raised to 360 °C, and equal molar selenium solution (in 2 ml in TOP) was quickly injected into the hot solvents. The mixture immediately changed color to orange-red, indicating quantum dot formation. The dots were refluxed for 30 minutes and cooled to 220 °C. A capping solution of 0.1 millimole dimethylzinc and hexamethyldisilathiane in 5 ml TOP was slowly added over a time course of 10 min at 220 °C and was refluxed for 30 min. The CdSe/ZnS dots formed have emission wavelength around 630-640 nm and excellent chemical and photo stability. The reaction mixture was then cooled to room temperature, and the dots were extracted with solvent methanol/hexane mixture (v/v 1:1).

**2.3 Polymer modification.** A triblock copolymer consisting of a poly-butylacrylate segment, a poly-ethylacrylate segment, and a poly-methacrylic acid segment was purchased from Sigma (St. Louis, MO). At a molecular weight of ~100,000 daltons, this polymer contains more than 1000 total monomer units, with a weight distribution of 23% methacrylic acid and 77% combined butyl and ethyl acrylates. For encapsulating QDs, about 25% of the free carboxylic acid groups were derivatized with octylamine (a hydrophobic side chain). Thus, the original polymer dissolved in dimethylformamide (DMF) was reacted with *n*-octylamine at a polymer/octylamine molar ratio of 1:40, using ethyl-3-dimethyl amino propyl carbodiimide (EDAC, 3-fold excess of *n*-octylamine) as a cross-linking reagent. The product yields were generally greater than 90% due to the high EDAC coupling efficiency in DMF (determined by a change of the free octylamine band in thin layer chromatography). The reaction mixture was dried with a ratovap (Rotavapor R-3000, Buchi Analytical Inc, Delaware). The resulting oily liquid was precipitated with water,

and was rinsed with water 5 times to remove excess EDAC and other by-products. After vacuum drying, the octylamine-grafted polymer was re-suspended in an ethanol / chloroform mixture, and was stored for use.

**2.4 QD surface modification and conjugation.** Using a 3:1 (v/v) chloroform/ethanol solvent mixture, TOPO-capped quantum dots were encapsulated by the amphiphilic tri-block polymer. A polymer-to-QD ratios of 5 -10 was used because molecular geometry calculations indicated that at least 4 polymer molecules would be required to completely encapsulate one quantum dot. Indeed, stable encapsulation (e.g., no aggregation) was not achieved at polymer/dot ratios less than 4:1. After vacuum drying, the encapsulated dots were suspended in a polar solvent (aqueous buffer or ethanol), and were purified by gel filtration. Standard procedures were then used to crosslink free carboxylic acid groups (ca. 100 on each polymer molecule) with amino-PEGs. Briefly, the polymer-coated dots were activated with 50 mM EDAC at pH 8 and reacted with amino-PEG at a QD/PEG molar ratio of 1:100 overnight. The QD bioconjugates were purified by column filtration or ultracentrifugation at 100,000 g for 30 min. After resuspension in PBS buffer (pH 7), trace amounts of aggregated particles were removed by centrifugation at 6000 g for 10 min.

**2.5 Fluorescence imaging.** In-vivo fluorescence imaging was accomplished by using a macro-illumination system (Lighttools Research, Encinitas, CA), designed specifically for small animal studies. True-color fluorescence images were obtained using dielectric long-pass filters (Chroma Tech, Brottletoro, VT) and a digital color camera (Optronics, Magnafire SP, Olympus America, Melville, NY).

Tissue sections were examined by using an inverted Olympus microscope (IX-70) equipped with a digital color camera (Nikon D1), a broad-band ultraviolet (330-385 nm) light source (100-W mercury lamp), and a long-pass interference filter (DM 400, Chroma Tech, Brattleboro, VT). Wavelength-resolved spectra were obtained by using a single-stage spectrometer (SpectraPro 150, Roper Scientific, Trenton, NJ).

**2.6 Cell, tissue, and whole-animal studies.** Mouse breast cancer cells (4T1) were used for implantation into immuno-compromised Balb/c nude mice. Using protocols approved by the Institutional Animal Care and Use Committee of Emory University, about  $0.5 \times 10^6$  tumor cells were injected into 6-8 weeks nude mice subcutaneously (Charles River, Wilmington, MA). Tumor growth was monitored daily until it reached the acceptable sizes. The mice were divided into 3 groups for control, unmodified dot and PEG dot studies. QDs were injected into the tail vein 6.0 nmol for each mouse. The mice were placed under anesthesia by injection of a Ketamine and Xylazine mixture intraperitoneally at a dosage of 95 mg/kg and 5 mg/kg, respectively. In a dark box, illumination was provided by fiber optic lighting, and a long pass filter was used to reject scattered excitation light and to pass Stokes-shifted QD fluorescence. Fluorescent images were recorded by a scientific-grade CCD camera. After whole-body imaging, the mice were sacrificed by CO<sub>2</sub> overdose. Tumor and major organs were removed and frozen for histological QD uptake and distribution studies. Tissue collections were cryosectioned into 5–10  $\mu\text{m}$  thickness sections, fixed with acetone at 0 °C, and examined with an epi-fluorescence microscope (Olympus IX70).

### 3. RESULTS AND DISCUSSION

**3.1 Probe design.** As schematically illustrated in **Figure 1**, core-shell CdSe-ZnS quantum dots are protected by a coordinating ligand (TOPO) and an amphiphilic polymer coating. Due to strong hydrophobic interactions between TOPO and the polymer hydrocarbon, these two layers “bond” to each other and form a hydrophobic protection structure that is resistant against hydrolysis and enzymatic degradation even under complex *in vivo* conditions (see below). In contrast to simple polymers and amphiphilic lipids used in previous studies<sup>6,7</sup>, we have used a high-molecular-weight (MW = 100 kD) copolymer with an elaborate ABC triblock structure and a grafted 8-carbon (C-8) alkyl side chain. This triblock polymer consists of a polybutylacrylate segment (hydrophobic), a polyethylacrylate segment (hydrophobic), a polymethacrylic acid segment (hydrophilic), and a hydrophobic hydrocarbon side chain. A key finding is that this polymer can disperse and encapsulate single TOPO-capped QDs via a spontaneous self-assembly process, similar to that reported by Ludwigs et al<sup>26</sup>. The resulted water-soluble QDs are highly stable against degradation, but form aggregations in acid pH and at high salt concentrations. To solve this problem and to improve particle biocompatibility, we used PEG chains with a molecular weight of 5,000 to cover the QD surface.

As a result, the QDs are protected to such a degree that their solubility and optical properties (e.g., absorption spectra, emission spectra, and fluorescence quantum yields) did not change in a broad range of pH (1 to 14) and salt conditions (0.01 to 1 M) or after harsh treatment with 1.0 M hydrochloric acid. Dynamic light scattering (DLS) measurement indicates that the assembled QD probes have a hydrodynamic radius of 10–15 nm. This value agrees with a compact probe structure consisting of a 5-nm QD core (2.5 nm radius), a 1-nm TOPO cap, a 2-nm thick polymer layer, and a 4–5-nm PEG layer.

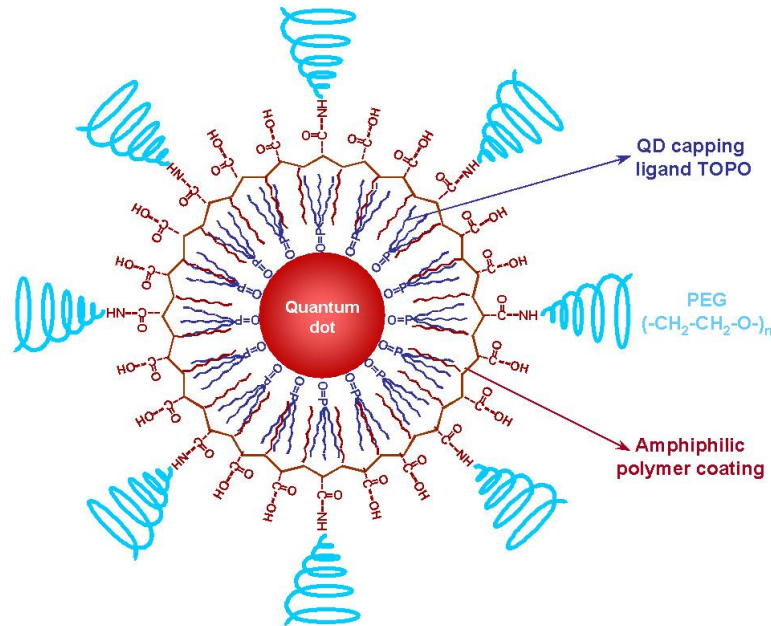


**Figure 1.** Schematic illustration of PEG conjugated quantum dots for *in vivo* cancer imaging. The structure of a long circulating QD probe shows the capping ligand TOPO, an encapsulating copolymer layer, and polyethylene glycol (PEG).

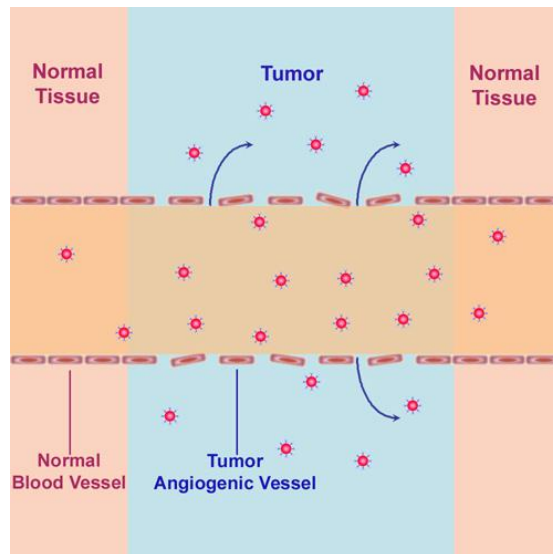


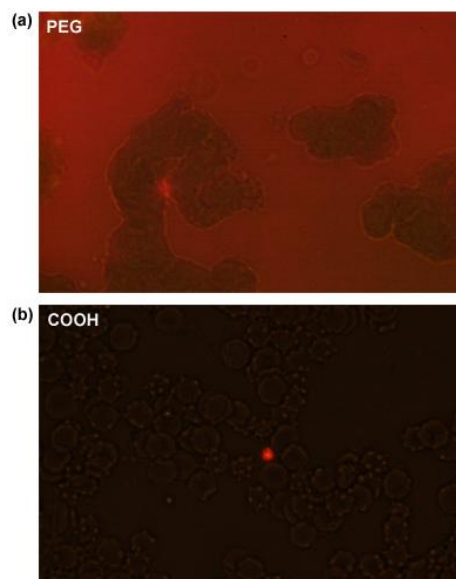
**Figure 2.** Schematic illustration showing enhanced permeation and retention (EPR) of nanometer-sized QD probes via leaky tumor vasculatures.

Based on the geometric/size constraints and the ligand coupling efficiencies, we have estimated that each dot contains ~200 TOPO molecules, 4–5 triblock copolymer molecules, and 10–20 PEG molecules. High-sensitivity fluorescence imaging showed “blinking” signals when a dilute solution ( $10^{-12}$  M) of the QD bioconjugate was spread on a glass surface. This blinking behavior is characteristic of single quantum systems such as single dye molecules and single QDs<sup>27</sup>, indicating that the triblock copolymer has efficiently dispersed the dots into single particles. Preliminary TEM results also revealed that the QD probes consisted of single particles, with little or no aggregation. It is worth noting, however, that QD blinking has no adverse implications for *in vivo* tumor imaging because the tumor cells are labeled with a large population (up to millions) of QDs, far from the single-dot regime.

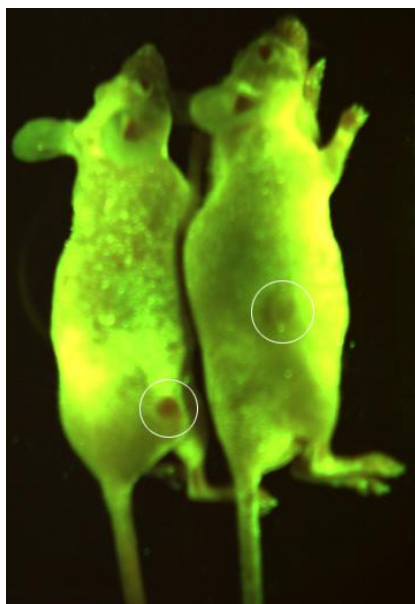
**3.2 Tumor targeting.** Through tail vein administration, QD probes are accumulated at tumor sites by a passive targeting mechanism (see Fig. 2). Macromolecules and nanometer-sized particles are accumulated preferentially at tumor sites through an enhanced permeability and retention (EPR) effect<sup>28</sup>. This effect is believed to arise from two factors: (a) angiogenic tumors which produce vascular endothelial growth factors (VEGF) that hyperpermeabilize tumor-associated neovasculatures and cause the leakage of circulating macromolecules and small particles; and (b) tumors lack an effective lymphatic drainage system, which leads to subsequent macromolecule or nanoparticle accumulation.

To achieve passive tumor targeting, long-circulating nanoparticle probes are needed to allow slow diffusion and accumulation at tumor sites through their leaky vasculatures. Therefore, we examined how functional groups on the QD surface would affect the probe circulation times *in vivo*. Figure 3 shows a comparison between water soluble QD with only carboxylic acid groups on the surface and PEG coated QDs. COOH dots were quickly removed by the RES system, with a plasma half-life of less than an hour. In contrast, the PEG coated QDs remained in the blood stream over a long period of time, with a plasma half-life of more than 5 hours. This long-circulating feature can be explained by the unique structural properties of QD nanoparticles. PEG coated QDs are in an intermediate size range – they are small and hydrophilic enough to slow down opsonization and reticuloendothelial uptake, while they are large enough to avoid renal filtration.

**Figure 3.** Fluorescence image of mouse blood samples obtained 24 hours after tail vein injection of QDs. PEG-coated QDs were still detectable in the blood circulation as shown by the red-orange fluorescence in (a), but the COOH dots were no longer observed, except for an aggregate in the image (b). Aggregated blood cells were observed as clots and small spheres.



We then proceed to examine the suitability of long-circulating QD probes for *in vivo* tumor imaging. Figure 4 depicts the true color fluorescence imaging results of mice injected with 6 nmole of QD-PEG and PBS buffer. At time 0 (right after injection), QD signals (red) were not detected in either group; however, 24 hours post-injection, the PEG coated QDs were detected at the tumor site as a red spot. This is expected due to the slow accumulation rate of QDs into solid tumors. Similar diffusion patterns have been observed by Weissleder and coworkers using magnetic nanoparticles. In comparison with specific targeting in which one type of probe only recognizes one target, the long-circulating probes are useful in broader applications because angiogenesis and disordered vasculatures occur in most tumors. The detection sensitivity could be further improved using wavelength-resolved spectral imaging, in which the strong autofluorescence is removed based on the spectral difference between QDs and mouse skin. We also noted that the current work using orange/red-emitting quantum dots is not optimized for tissue penetration or imaging sensitivity. Extensive work in tissue optics has shown deep tissue imaging (millimeters to centimeters) requires the use of far-red and near-infrared light in the spectral range of 650–900 nm<sup>29</sup>. This wavelength range provides a “clear” window for *in vivo* optical imaging because it is separated from the major absorption peaks of blood and water<sup>30</sup>. Based on tissue optical calculations, we estimate that the use of near-infrared-emitting quantum dots could improve the tumor imaging sensitivity by at least 10-fold. Toward this goal,



recent research has prepared a new class of alloyed semiconductor quantum dots consisting of cadmium selenium telluride, with tunable fluorescence emission up to 850 nm<sup>31</sup>. Together with core-shell CdTeCdSe type-II materials<sup>32</sup>, the use of near-infrared-emitting QDs should bring major improvements in tissue penetration depth and cell detection sensitivity.

**Figure 4.** Fluorescence imaging of QD-PEG conjugates in live animals harbored with 4T1 tumor xenografts. Dark-red fluorescence signals indicate a tumor growing in a live mouse (left). Control studies by injecting PBS buffers showed no QD fluorescence signals (right). The images were obtained 24 hour post injection.

**3.3 Biodistribution.** To confirm the behavior of QD-PEG probes in living animals, we examined their organ uptake and distribution as well as the effect of particle surface modifications. **Figure 5** shows QD uptake and retention took place primarily in the tumor, liver and the spleen. Little or no QD accumulation was observed in the brain, the heart, the kidney, or the lung (data not shown). As seen from the characteristic red fluorescence of

quantum dots, QDs with only COOH groups were not observed in tumors, indicating nonspecific RES uptake and rapid blood clearance. For polymer-encapsulated QDs with surface PEG groups, the rate of RES uptake was reduced and the length of blood circulation was improved, leading to slow accumulation of the nanoparticles in the tumors, although nonspecific liver and spleen uptake was still apparent.

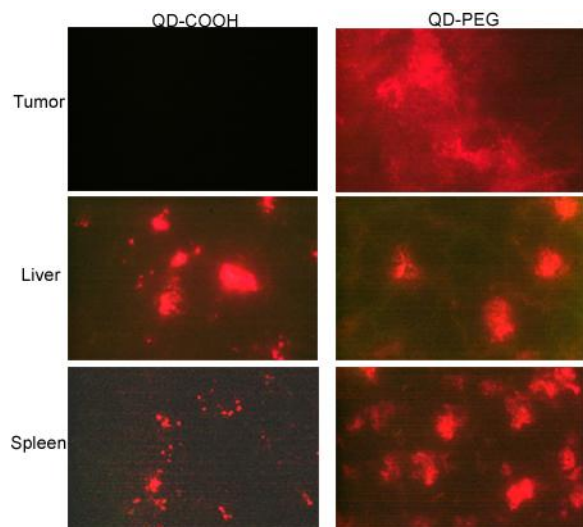


**Figure 5.** Histological examination of QD uptake, retention, and distribution in organs and in 4T1 tumor xenografts maintained in athymic nude mice. Left column: QD coated with carboxylic acid groups. Right column: QD with surface coated with PEG groups. All images were obtained from 5–10  $\mu\text{m}$ -thin tissue sections on an epi-fluorescence microscope. QDs were detected by their characteristic red fluorescence.

**3.4 Multicolor imaging.** We have further explored multicolor *in vivo* imaging with QD-encoded microbeads. For this purpose, three samples of 0.5- $\mu\text{m}$  polymer beads, each doped with green, yellow or red QDs, were injected into a mouse model at three different locations, similar to previous reports of using fluorescent beads for cell differentiation and trafficking studies<sup>33</sup>. Due to the unusually large Stokes shifts and broad excitation profiles of QDs, all three colors were observed simultaneously in the same mouse and with a single light source (**Fig. 6**).

**3.5 Toxicity.** At the present, little is known about the mechanism of metabolism or clearance of QD probes injected into living animals. For the polymer-encapsulated QDs, chemical or enzymatic degradations of the semiconductor cores are unlikely to occur. But the polymer-protected QDs might be cleared from the body by slow filtration and excretion through the kidney. This and other possible mechanisms need to be examined carefully because potential human use of semiconductor QDs will require a detailed knowledge of their eventual disposition after injection.

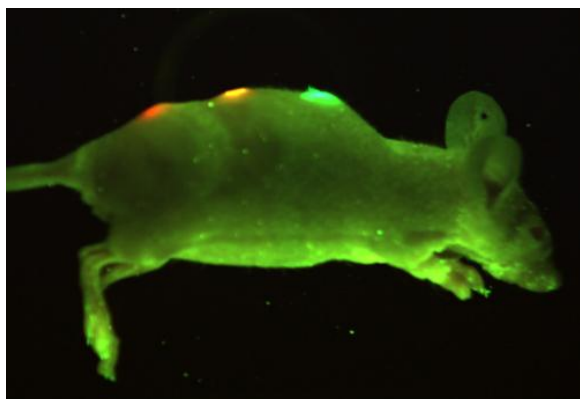


**Figure 6.** Simultaneous *in vivo* imaging of multicolor QD-encoded microbeads injected in a living mouse. QD-encoded microbeads (0.5  $\mu\text{m}$  diameter) emitting green, yellow, or red light were injected subcutaneously (about one bead in each color) at three adjacent locations on a host animal. The animal imaging data were acquired with tungsten or mercury lamp excitation and a filter set designed for GFP fluorescence.

#### 4. CONCLUSION

In conclusion, we have developed a new class of polymer-encapsulated and PEG-linked QD probes for cancer imaging *in vivo*. These probes are bright, stable, and have a versatile triblock copolymer structure that is well suited for

conjugation to additional diagnostic and therapeutic agents. *In vivo* imaging results indicate the QD probes can be targeted to tumor sites through the EPR effect. The use of spectral imaging machine and near-infrared-emitting quantum dots should improve both the tissue penetration depth and imaging sensitivity. We envision that quantum dots might be integrated with targeting, imaging, and therapeutic agents to develop “smart” nanostructures for noninvasive imaging, diagnosis, and treatment of cancer, cardiovascular plaques, and neurodegenerative disease.

#### 5. ACKNOWLEDGEMENTS

This work was supported by grants from the National Institutes of Health (R01 GM60562, P20 GM072069, and R01 CA108468), the Georgia Cancer Coalition (Distinguished Cancer Scholar Award), and the Coulter Translational Research Program at Georgia Tech and Emory University.

#### 6. REFERENCES

1. Chan, W.C.W. *et al.* “Luminescent QDs for multiplexed biological detection and imaging”, *Curr. Opin. Biotechnol.* **13**, 40–46, 2002.
2. Bruchez, M. Jr., Moronne, M., Gin, P., Weiss, S. & Alivisatos, A. P. “Semiconductor nanocrystals as fluorescent biological labels”, *Science* **281**, 2013–2015, 1998.
3. Chan, W.C.W. & Nie, S.M. “Quantum dot bioconjugates for ultrasensitive nonisotopic detection”, *Science* **281**, 2016–2018, 1998.
4. Mattoussi, H. *et al.* “Self-assembly of CdSe–ZnS QDs bioconjugates using an engineered recombinant protein”, *J. Am. Chem. Soc.* **122**, 12142–12150, 2000.
5. Akerman, M.E., Chan, W.C.W., Laakkonen, P., Bhatia, S.N. & Ruoslahti, E. “Nanocrystal targeting *in vivo*”, *Proc. Natl. Acad. Sci. U. S. A* **99**, 12617–12621, 2002.
6. Dubertret, B. *et al.* “*In vivo* imaging of QDs encapsulated in phospholipid micelles”, *Science* **298**, 1759–1762, 2002.
7. Wu, X.Y. *et al.* “Immunofluorescent labeling of cancer marker Her2 and other cellular targets with semiconductor QDs”, *Nat. Biotechnol.* **21**, 41–46, 2003.
8. Jaiswal, J.K. Mattoussi, H., Mauro, J.M. & Simon, S.M. “Long-term multiple color imaging of live cells using quantum dot bioconjugates”, *Nat. Biotechnol.* **21**, 47–51, 2003.
9. Larson, D.R. *et al.* “Water-soluble quantum dots for multiphoton fluorescence imaging *in vivo*”, *Science* **300**, 1434–1436, 2003.
10. Ishii, D. *et al.* “Chaperonin-mediated stabilization and ATP-triggered release of semiconductor nanoparticles”, *Nature* **423**, 628–632, 2003.
11. Medintz, I.L. *et al.* “Self-assembled nanoscale biosensors based on quantum dot FRET donors”, *Nat. Mater.* **2**, 630–639, 2003.
12. Dahan, M. *et al.* “Diffusion dynamics of glycine receptors revealed by single-quantum dot tracking”, *Science* **302**, 441–445, 2003.

13. Rosenthal, S.J. et al. "Targeting cell surface receptors with ligand-conjugated nanocrystals", *J. Am. Chem. Soc.* **124**, 4586–4594, 2002.
14. Niemeyer, C.M. "Nanoparticles, proteins, and nucleic acids: biotechnology meets materials science", *Angew. Chem. Int. Ed.* **40**, 4128–4158, 2001.
15. Alivisatos, A.P. "Semiconductor clusters, nanocrystals, and quantum dots", *Science* **271**, 933–937, 1996.
16. Han, M.Y., Gao, X.H., Su, J.Z. & Nie, S.M. "Quantum dot-tagged microbeads for multiplexed optical coding of biomolecules", *Nat. Biotechnol.* **19**, 631–635, 2001.
17. Gao, X.H. & Nie, S.M. "Doping mesoporous materials with multicolor quantum dots", *J. Phys. Chem. B.* **107**, 11575–11578 (2003); "Quantum dot-encoded mesoporous beads with high brightness and uniformity: rapid readout using flow cytometry", *Anal. Chem.* **76**, 2406–2410, 2004.
18. Josephson, L., Kircher, M.F., Mahmood, U., Tang, Y. & Weissleder R. "Near-infrared fluorescent nanoparticles as combined MR/optical imaging probes", *Bioconjug. Chem.* **13**, 554–560, 2002.
19. Gao, X.H. & Nie, S.M. "Molecular profiling of single cells and tissue specimens with quantum dots", *Trends Biotechnol.* **21**, 371–373 (2003). Jovin, T.M. "Quantum dots finally come of age", *Nature Biotechnol.* **21**, 32–33, 2003.
20. Lim, Y.T. *et al.* "Selection of quantum dot wavelengths for biomedical assays and imaging", *Mol. Imaging* **2**, 50–64, 2003.
21. Ballou, B., Lagerholm, B. C., Ernst, L. A., Bruchez, M. P. & Waggoner, A. S. "Noninvasive imaging of quantum dots in mice," *Bioconjug. Chem.* **15**, 79–86, 2004.
22. Kim, S. et al. "Near-infrared fluorescent type II quantum dots for sentinel lymph node mapping", *Nature Biotechnol.* **22**, 93–95, 2004.
23. Gao X, Cui Y, Levenson RM, Chung LW, Nie S., "In vivo cancer targeting and imaging with semiconductor quantum dots", *Nature Biotechnol.* **22**, 969–976, 2004
24. Peng, Z.A. & Peng, X. "Formation of high-quality CdTe, CdSe, and CdS nanocrystals using CdO as precursor", *J. Am. Chem. Soc.* **123**, 183–184, 2001. Qu, L.H. Peng, Z.A. & Peng, X. "Alternative routes toward high quality CdSe nanocrystals", *Nano Lett.* **1**, 333–337, 2001.
25. Hines MA and Guyot-Sionnest P, "Synthesis and Characterization of Strongly Luminescing ZnS-Capped CdSe Nanocrystals", *J. Phys. Chem.*, 100, 468 – 471, 1996.
26. Ludwigs, S. *et al.* "Self-assembly of functional nanostructures from ABC triblock copolymers", *Nat. Mater.* **2**, 744–747, 2003.
27. Nirmal, M. *et al.* "Fluorescence intermittency in single cadmium selenide nanocrystals", *Nature* **383**, 802–804, 1996. Empedocles, S.A. & Bawendi, M.G. "Quantum-confined stark effect in single CdSe nanocrystallite quantum dots", *Science* **278**, 2114–2117, 1997.
28. Jain, R.K. "Transport of molecules, particles, and cells in solid tumors", *Ann. Rev. Biomed. Eng.* **1**, 241–263, 1999; Jain, R.K. "Delivery of molecular medicine to solid tumors: lessons from in vivo imaging of gene expression and function", *J. Control. Release* **74**, 7–25, 2001.
29. Cheong, W. F., Prael, S. A. & Welch, A. J. "A review of the optical properties of biological tissues," *IEEE J. Quantum Electronic* **26**, 2166–2185, 1990.
30. Ntziachristos, V., Bremer, C. & Weissleder, R. "Fluorescence imaging with near-infrared light: new technological advances that enable *in vivo* molecular imaging", *Eur. Radiol.* **13**, 195–208, 2003.
31. Bailey, R.E. and Nie, S.M. "Alloyed semiconductor QDs: tuning the optical properties without changing the particle size", *J. Am. Chem. Soc.* **125**, 7100–7106, 2003.
32. Kim, S., Fisher, B., Eisler, H. J. & Bawendi, M. G. "Type-II quantum dots: CdTe/CdSe (core/shell) and CdSe/ZnTe (core/shell) heterostructures", *J. Am. Chem. Soc.* **125**, 11466–11467, 2003.
33. Randolph, G.J., Inaba, K., Robbiani, D.F., Steinman, R.M. & Muller, W.A. "Differentiation of phagocytic monocytes into lymph node dendritic cells *in vivo*", *Immunity* **11**, 753–761, 1999.